Acta Cryst. (1978). A**34**, 922–931

Structural Studies by High-Resolution Electron Microscopy: Intergrowth of ReO_3- and Tetragonal Tungsten Bronze-Type Structures in the System Nb_2O_5–WO_3

BY SUMIO IIJIMA

Department of Physics, Arizona State University, Tempe, Arizona 85281, *USA*

(*Received* 7 *February* 1978; *accepted* 11 *May* 1978)

With high-resolution electron microscopy new crystal structures were found in the binary system of Nb_2O_5–WO_3 oxides. The compounds are proposed to have the mole ratios $4Nb_2O_5.22WO_3$ and $4Nb_2O_5.50WO_3$. The crystal structures are ascribed to intimate intergrowths of two known structures, the ReO_3 type and tetragonal tungsten bronze type. The latter grows coherently in the host lattice of the former, forming regularly arranged slabs. The coherent intergrowth of the tetragonal tungsten bronze structures is described as the 'rotation operation' on the ReO_3-type structure.

Introduction

Compounds in the binary system of Nb_2O_5–WO_3 oxides have been intensively studied. According to the studies on the phase diagram of this system by Roth & Wadsley (1965), the compounds are grouped into three different structure types: the 'block structures' occurring in the composition range of O/M (oxygen/metal ratio) = 2·50–2·66, the 'Magnéli phases' in the WO_3-rich region of O/M = 2·90–3·00, and in the range of O/M = 2·66–2·90 the tetragonal tungsten bronze-type structure (hereinafter abbreviated TTB type). For the TTB type, two ordered structures $4Nb_2O_5.9WO_3$ and $2Nb_2O_5.7WO_3$ were found. The block structures and the Magnéli phases having the ReO_3 type as a basic structure contain the crystallographic shear structures as a common structural component where the individual metal–oxygen octahedra are linked with their neighboring octahedra by edge sharing instead of corner sharing in the basic structure of the ReO_3 type. In the Magnéli phases the crystallographic shear planes are arranged one-dimensionally, forming slabs of the ReO_3 type, while in the block structures the crystallographic shear planes are arranged two-dimensionally, forming columns of the ReO_3 type. A slight change in composition results in rearrangement of the crystallographic shear planes and thus a slightly different structure from one compound to another, so that a homologous series of the compounds is formed (Wadsley & Andersson, 1970).

The structure of $2Nb_2O_5.7WO_3$ was determined from the study of the high-resolution electron micrographs of crystals having a nominal composition of $19Nb_2O_5.63WO_3$ (Iijima & Allpress, 1974*a*) and was found to result from an intergrowth of the two different structures of ReO_3 type and the TTB type. It was proposed that since the small domains of the ReO_3-type structure are intergrown coherently with the TTB type in $2Nb_2O_5.7WO_3$, a transformation of this structure from the ReO_3 type to the TTB type, which occurs in solid-state reactions, would be conceivable by a periodic application of the rotation of the groups of the corner-shared octahedra to the ReO_3 type. Direct evidence of the rotation which causes formation of single elements of the TTB-type structure in some regions of the ReO_3 type has been demonstrated by Iijima & Allpress (1974*b*). This was observed often in disordered regions of crystals having a nominal composition of $19Nb_2O_5.63WO_3$. More general considerations on structural relations between the ReO_3 type and some 'bronze' and 'tunnel' structures formed by a simple geometrical rotation operation on the ReO_3 type were discussed by Hyde & O'Keeffe (1973).

In the present paper we report new structures in the binary system of Nb_2O_5–WO_3 that have intergrowths of the ReO_3 type and the TTB type similar to that of $2Nb_2O_5.7WO_3$. Compared with the structure of $2Nb_2O_5.7WO_3$, the new structures are composed predominantly of regions of ReO_3 type and show less effect of the rotation operation on the ReO_3 type. The new structures will be discussed in comparison with the crystallographic shear structures. Also, a reaction mechanism will be considered for converting the ReO_3 type to the intergrowth structures in the solid state.

Experimental

The sample, having nominal composition $19Nb_2O_5.63WO_3$, studied in the present work was the same as that studied by Iijima & Allpress (1974*b*), and was provided by Dr R. S. Roth and the late A. D. Wadsley (Roth & Wadsley, 1965). It was prepared by heating a mixture of $19Nb_2O_5$ and $63WO_3$ in a sealed

platinum capsule at 1620 K for 18 h and quenching the product.

The small fragments of the crystals were collected on the perforated carbon films on the copper specimen grids for the electron microscope. Thin edges of the fragments were sought and their crystal orientations were aligned in a goniometer stage so as to give the (*hk*0) reflections referring to the structure of $2Nb_2O_5.7WO_3$. The images of the crystals were taken by a JEM-100B electron microscope at 100 keV using a pointed filament.

Conditions under which the images were taken will be reported in a paper by Iijima & O'Keefe (1978), in which detailed comparison of the experimental and theoretically calculated images of the imperfect crystals described in the present paper will be made in terms of the electron optical effects and electron diffraction.

The crystals prepared from a nominal composition $19Nb_2O_5.63WO_3$ contain predominantly regions of $2Nb_2O_5.7WO_3$ but also show considerable disorder in linkage of the metal–oxygen octahedra. The rearrangement of the octahedra in the disordered regions which we shall be concerned with in the present study is perfectly regular in a certain crystallographic orientation coincident with the [001] direction of $2Nb_2O_5.7WO_3$. Such two-dimensional disorders are known to be quite common in the compounds in the system Nb_2O_5–WO_3 and the nature of the disorders has been studied previously using high-resolution electron microscopy in relation to the nonstoichiometry of the compounds (Iijima & Allpress, 1974*a*,*b*; Iijima, 1975*a*; Iijima & Cowley, 1978).

Fig. 1(*a*) shows a two-dimensional high-resolution electron micrograph from a disordered region of the thin crystal having nominal composition $19Nb_2O_5.63WO_3$. The micrograph was recorded under the condition of the 'optimum focus' of the microscope, so that its image contrast reflects approximately the crystal potential projected along the incident electron beam direction (O'Keefe, Buseck & Iijima, 1978). As reported by Iijima & Allpress (1974*b*), the region has been described as basically composed of two different crystal structures, the ReO_3 type (seen as a

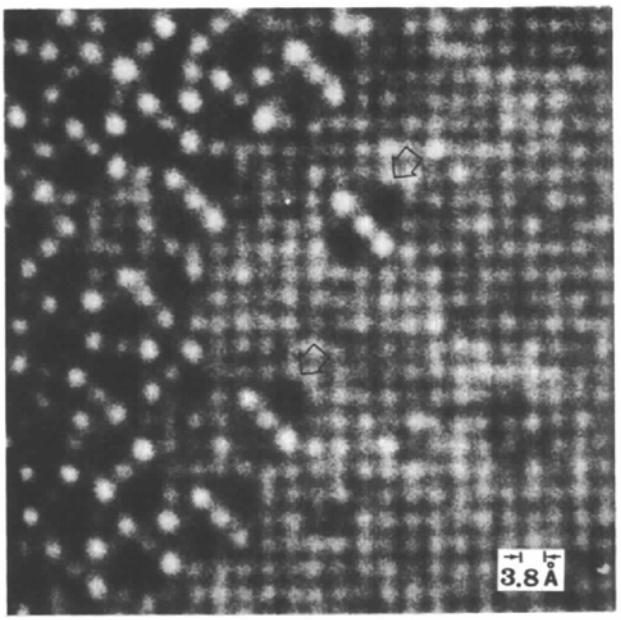

(*a*)

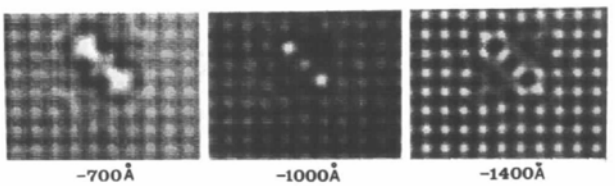

(*b*)

Fig. 1. (*a*) A high-resolution electron micrograph showing a disordered arrangement of the atoms in a crystal having a nominal composition $19Nb_2O_5.63WO_3$. The region on the left of the image has a tetragonal tungsten bronze-type structure (Fig. 2*b*). The square patterns shown by arrows are described by coherent intergrowth of a single unit cell of the TTB-type structure with the ReO_3 type. The dark contrast appearing inside the region of the TTB element corresponding to the pentagonal tunnels (Fig. 2*b*) indicates that they are occupied by metal atoms. (*b*) A through-focus series of images calculated for the model structure of the TTB element with two pentagonal tunnels occupied (Fig. 2*b*). The 'optimum focus' image (−1000 Å) resembles the experimental images and thus the assumed structure for the TTB element is shown to be reasonable (Iijima & O'Keefe, 1978).

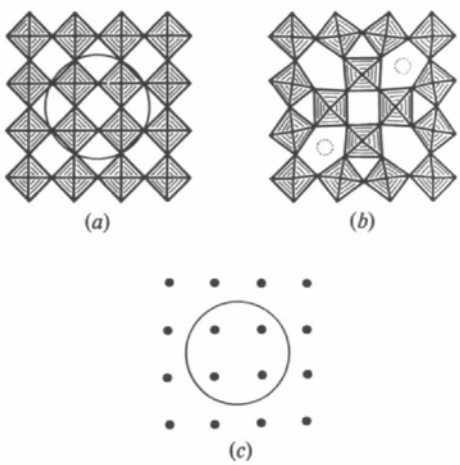

(*a*) (*b*) (*c*)

Fig. 2. (*a*) Idealized model for the ReO_3-type structure projected along the direction of one of the cube axes. Hatched squares represent metal–oxygen octahedra that are connected to adjacent octahedra by corner sharing. (*b*) Model of the TTB-type structure, that is related geometrically to the ReO_3 type. A rotation operation on the ReO_3 type creates this structure, *i.e.* 45° rotation of the four octahedra inside the circle drawn in Fig. 2(*a*), resulting in the generation of four pentagonal tunnels. Some of them may be occupied as seen in Fig. 1(*a*). (*c*) Simplified designation of the ReO_3-type structure which is used in describing the faulted structure of Fig. 7.

region where the fringe patterns intersect orthogonally) and the TTB type (on the left-hand side of the image). The dark areas of the fringe pattern appearing in the ReO_3 type region correspond to the individual columns of the metal atom positions in the corner-shared octahedra which are separated by 3·8 Å both horizontally and vertically. The idealized model for the ReO_3 type viewed along one of the cube axes is illustrated in Fig. 2(*a*), where each hatched square represents a metal–oxygen octahedron which repeats in the direction perpendicular to the plane of the page.

The square patterns (indicated by arrows in Fig. 1*a*) appearing in the region of the ReO_3 type are explained as the elements of the TTB type (Fig. 2*b*). They fill up the entire region of the disordered $4Nb_2O_5.9WO_3$ which is seen on the left of Fig. 1(*a*). From a comparison of the ReO_3 type with the TTB type it is evident that the two structures are related geometrically to each other by the rotation operation. This can be seen by rotating, within the plane of the page, four octahedra (encircled in Fig. 2*a*) located near the center by 45°. The operation results in the formation of four large pentagonal tunnels and small triangular tunnels.

The linear arrangement of three white spots appearing in each square pattern in the image suggests that there are three empty tunnels. Two of the four pentagonal tunnels however are filled with metal–oxygen strings perpendicular to the plane of the page and thus these regions are imaged as dark blobs. A through-focus series of the images of the model structure of a single TTB-type element in the ReO_3-type host lattice (Fig. 2*b*) calculated theoretically using an *artificial superstructure method* is shown in Fig. 1(*b*). The experimental image of the TTB-type element agrees with the calculated image of −1000 Å defocus. The details will be reported elsewhere (Iijima & O'Keefe, 1978). The occupation of the pentagonal tunnels, similar to the observation mentioned above, was reported in some ordered structures such as $4Nb_2O_5.9WO_3$ (Sleight, 1966) and $2Nb_2O_5.7WO_3$ (Iijima & Allpress, 1974*a*). The metal/oxygen ratio in the region of the elements of the TTB type with two pentagonal tunnels occupied becomes $MO_{2.636}$, compared with MO_3 for the ReO_3 type. Occurrence of the TTB-type elements therefore is attributed to the reduction of the host ReO_3-type structure. In other words, such a segregation of both metal and oxygen ions into the columns causes the nonstoichiometry of the MO_3 host structure.

Fig. 3 shows a dark-field image at a lower magnification taken from the same batch of the sample. The region showing a regular arrangement of the square patterns in the top of the image has the tetragonal structure of $2Nb_2O_5.7WO_3$ ($a_1 = a_2 = 24$ Å, $c = 3{\cdot}8$ Å, space group $P4$). This is the most common structure in the present sample of $19Nb_2O_5.63WO_3$. Some antiphase boundaries, indicated by large arrows, are recognized in this region.

Another structure that we wish to describe below

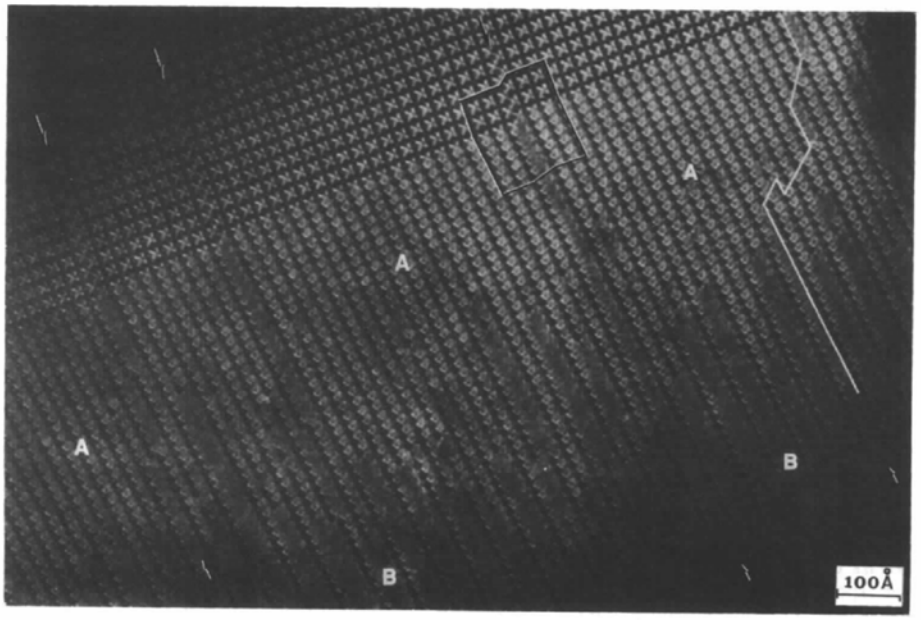

Fig. 3. A dark-field electron micrograph taken from a crystal of $19Nb_2O_5.63WO_3$. The upper region of square patterns has the tetragonal structure of $2Nb_2O_5.7WO_3$ and contains some antiphase boundaries (large arrows). The crystal structures in the regions shown by *A* and *B* are intergrowths of the ReO_3 type and the TTB type. Dark lines in these regions correspond to the slabs of the TTB type. The spacing of the slabs in region *A* becomes doubled in region *B* because of termination of alternate slabs. Some stacking faults (arrows) and their displacements (shown by white lines) are also recognized in these regions.

extends from the region of $2Nb_2O_5.7WO_3$, which is separated by a distinct boundary running from the upper right corner to the middle left of the image. The boundary has a crystallographic orientation parallel to the a_1 or a_2 axis of $2Nb_2O_5.7WO_3$. This new structure appears to be due to ordering of some types of the extended planar defects or slabs. Two different periodicities in the regular arrays of the slabs can be recognized in regions marked by *A* and *B* in Fig. 3. The spacing between the adjacent slabs in the region *A* is a half of that in the region *B*. Omission of the slabs in every other row in *B* results in regular arrays with double spacing.

Besides these two regular spacings, a third type of spacing can also be seen occasionally in some regions (indicated by small arrows near the bottom). These disturb the regular arrays of the slabs and thus these regions are considered as stacking faults. They appear to originate from the antiphase boundaries in the region of $2Nb_2O_5.7WO_3$. The occasional steps or jogs in the individual planar defects cause shifts of the stacking faults to the side (see the lines drawn in the upper right corner of Fig. 3). The nature of the stacking faults and the interface of the two structures have been discussed (Iijima & Allpress, 1974*b*) and will be discussed further in the later section.

An electron diffraction pattern corresponding to the image of Fig. 2 is reproduced in Fig. 4(*a*). This was found to originate from four different types of reciprocal lattice, which are schematically illustrated in Fig. 4(*b*). A large square net of diffraction spots with strong intensities (shown by large open circles) corresponds to the ReO_3-type structure. A small square arrangement of spots (shown by small open circles) is attributed to the region of the tetragonal structure of $2Nb_2O_5.7WO_3$. The other two groups of the spots (shown by large and small solid circles) might result from the regions where the planar defects are regularly arranged. Since the positions of some of these weak reflections coincide with those of the ReO_3 type, it can be expected that the new structures are predominantly ReO_3 type, and the regularly arranged planar slabs are coherently intergrown in the host ReO_3-type lattice, *i.e.* superlattices of the ReO_3 type.

Accordingly, the reciprocal-lattice vectors of the unit cell of the new structure could be derived immediately with reference to those of the sublattice of the ReO_3 type (a_R = 3·8 Å). They are measured to be $a^* = (1/14)[210]^*_R$ or $(1/28)[210]^*_R$, $c^* = (1/14)[130]^*_R$ and $\beta^* = 81{\cdot}9°$, where the suffix *R* denotes the lattice of the ideal structure of the ReO_3 type. Assuming that the b^* axis of the unit cell is perpendicular to the plane of the page in Fig. 4(*b*), the unit-cell dimensions are calculated to be a = 24·03 or 48·06, b = 3·8, c = 16·99 Å

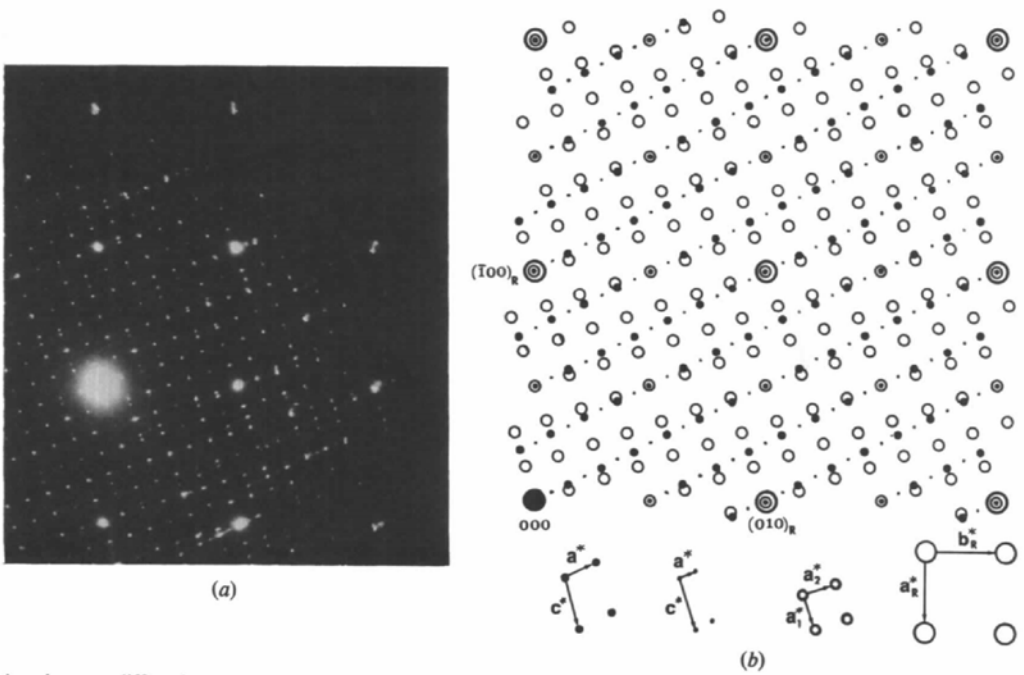

(*a*) (*b*)

Fig. 4. (*a*) An electron diffraction pattern corresponding to the region shown in Fig. 3, which contains four different reciprocal-lattice sections. (*b*) Schematic illustration of the diffraction spots in (*a*). Two sets of square arrangements of the spots correspond to the tetragonal structure of the ReO_3 type (large open circles) and $2Nb_2O_5.7WO_3$ (small open circles). The other two sets were found to be from the intergrown structures from the regions *A* and *B* shown in Fig. 3. The reciprocal-lattice points of the ReO_3 type are common to those for the other three structures, so that they can be intergrown coherently with the ReO_3 type and thus are considered as its superstructures.

and $\beta = 98{\cdot}13°$. The symmetry of the structure is monoclinic and its two-dimensional space group is $P2$.

Fig. 5 shows a bright field 'structure image' corresponding to a portion of Fig. 3. As we have expected from observations of the electron diffraction patterns of Fig. 4 and the lower-magnification micrograph of Fig. 3, the host substructure is indeed the ReO_3 type, which is seen as a perpendicularly intersecting fringe pattern similar to the one in Fig. 1(*a*). The regions of the ReO_3 type are separated by regularly arranged planar faults or slabs. Furthermore, the micrograph reveals that the individual extended planar faults consist of regular arrays of the elements of the TTB-type cells with two of the four pentagonal tunnels in the TTB-type cells occupied regularly, as in the case of the isolated TTB-type element shown in Fig. 1(*a*). The photograph also proves that the new structures are intimate coherent intergrowths of two structures of ReO_3 type and the TTB type.

The spacings of the adjacent slabs of the TTB type cells can be derived directly by referring to the fringe spacing of 3·8 Å appearing in the ReO_3-type regions. They are in accord with those we obtained from the electron diffraction data of Fig. 4. Two different spacings are recognized in the micrograph (indicated by *A* and *B*). A simplified model for one of the structures projected along the [010] direction (a = 24·01 and c = 16·99 Å), which has been derived from the structure image of Fig. 5, is illustrated and the unit cell is outlined in Fig. 6(*a*). The hatched squares represent the individual metal–oxygen octahedra that are linked by their corner-sharing. The pentagonal

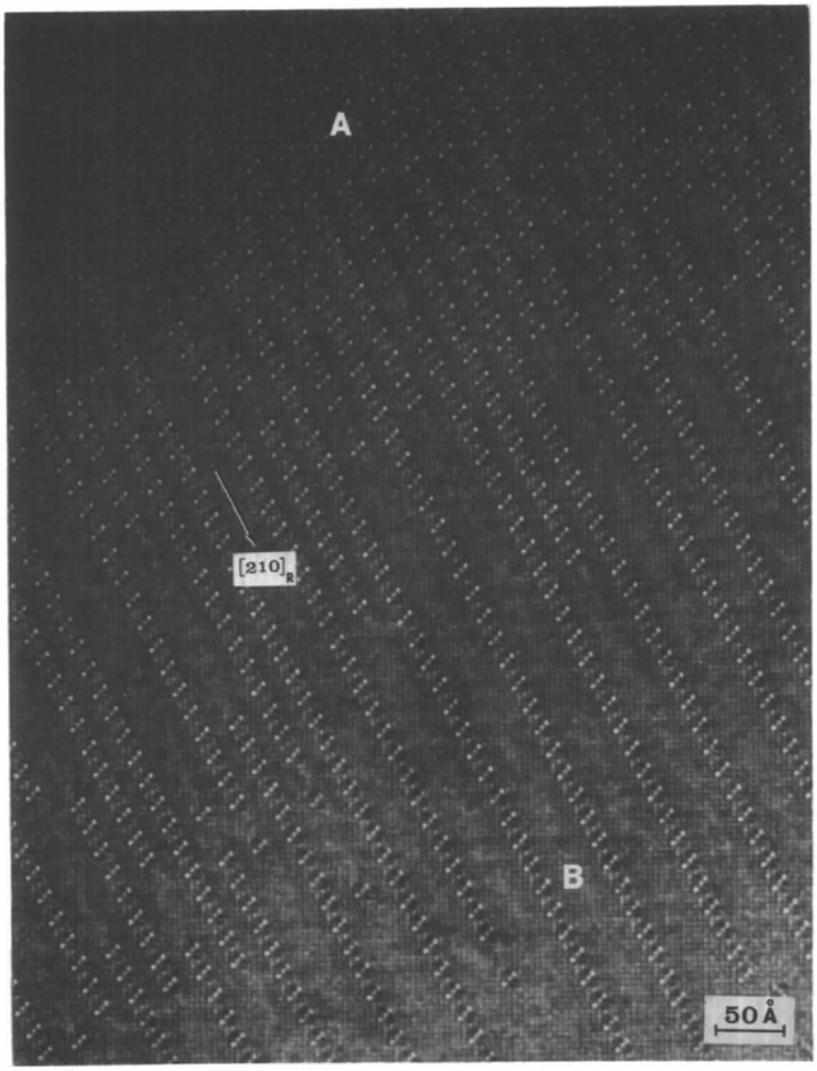

Fig. 5. A high-resolution electron micrograph taken from a portion of the same crystal as that of Fig. 3. The slabs giving the dark lines in Fig. 3 consist of regular arrays of the TTB-type elements shown in Fig. 1. The slabs are extended in the $[210]_R$ direction of the ReO_3 type. The termination of the slabs causes two homologous structures; $4Nb_2O_5 . 22WO_3$ (region *A*) and $4Nb_2O_5 . 50WO_3$ (region *B*).

tunnels occupied by the metal–oxygen strings are shown by the open circles. The orientation of the extended slabs lies parallel to $[210]_R$, which agrees with the observation of the electron diffraction pattern. For the structure having a doubled a axis (48·02 Å), the slabs of the TTB type are missing in every other row and they are replaced by the ReO_3 type.

The content of metal and oxygen atoms for the small unit cell is $28 \times MO_3$ (octahedra) + $2 \times MO$ (tunnels) = $M_{30}O_{86}$ = $MO_{2.867}$. For the doubled unit-cell structure $56 \times MO_3 + 2 \times MO = M_{58}O_{170} = MO_{2.931}$ is obtained. The former composition corresponds to the mole ratio $4Nb_2O_5.22WO_3$ in the system Nb_2O_5–WO_3 and the latter becomes $4Nb_2O_5$–$50WO_3$. These compositions are compared in Table 1 with the other structures in the WO_3-rich region in the system Nb_2O_5–WO_3. For the purpose of comparison the table includes also the Magnéli phases. The Magnéli phases whose compositions are represented by a general formula $(Mo,W)_nO_{3n-1}$, where n = 8–14, are described by regular arrangements of the one-dimensional crystallographic shear planes in the ReO_3 type (Magnéli, 1953). The range of compositions for the one-dimensional shear-structure compounds extends from 2·875 to 2·929 and thus it overlaps partly those of the new structures. Allpress (1972) examined the structures of the compounds having compositions $WO_3.xNb_2O_5$ (x = 0·03–0·09, or the O/M ratio = 2·881–2·972) and concluded that the structures of these compounds are the ReO_3 type modulated by the one-dimensional crystallographic shear planes. He also found that some of the specimens contain regular arrangements of the crystallographic shear planes. The table indicates that the range of the compositions for the intergrowth structures of $2Nb_2O_5.7WO_3$, $4Nb_2O_5.22WO_3$ and $4Nb_2O_5.50WO_3$ extends from 2·818 to 2·931 and lies between that of the pure TTB type and the crystallographic shear structures. As the oxygen content in the system increases, the structures of the compounds in the system Nb_2O_5–WO_3 tend to increase in amount of regions of the ReO_3 type. Actually, such a gradual change in composition is observed in Fig. 3: the structures change as $2Nb_2O_5.7WO_3 \rightarrow 4Nb_2O_5.22WO_3 \rightarrow 4Nb_2O_5.50WO_3$ (from the top to the bottom). This indicates that the crystals examined in the present study are non-equilibrium products.

Table 1. *The structures of the compounds in the* WO_3–Nb_2O_5 *system*

Ordered intergrowths of TTB-type and ReO_3-type structure were found in the present study.

Compounds	Content of ideal unit cell	Range of composition O/M	Crystal structure
Block structure		2·5–2·66	Two-dimensional CS structure
$4Nb_2O_5.9WO_3$	$B_{17}O_{47}$	2·765	TTB
$2Nb_2O_5.7WO_3$	$B_{11}O_{31}$	2·818	TTB + ReO
$4Nb_2O_5.22WO_3$	$B_{30}O_{86}$	2·867	TTB + ReO
$4Nb_2O_5.50WO_3$	$B_{58}O_{170}$	2·931	TTB + ReO
Magnéli phases $(Mo,W)_nO_{3n-1}$ and related structures		2·875–3·00	One-dimensional CS structure

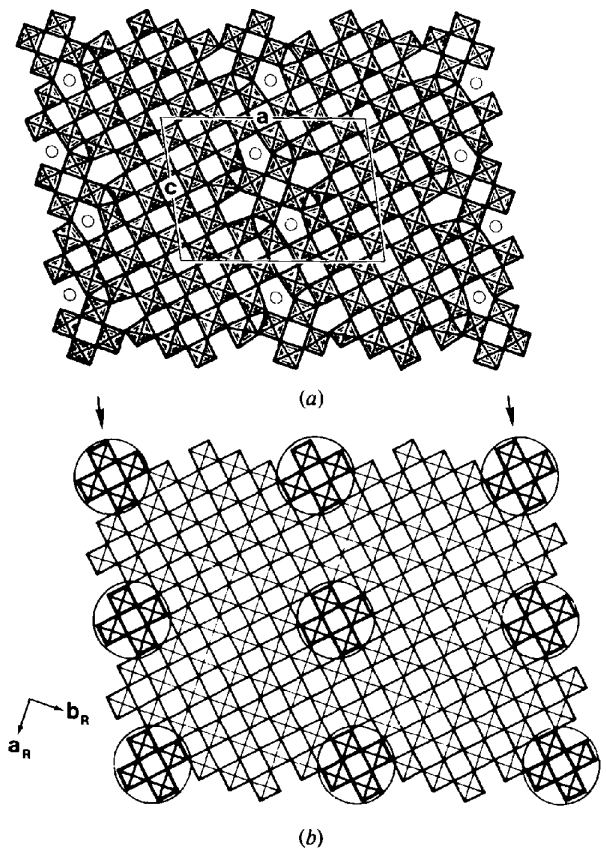

Fig. 6. (*a*) Idealized model for the crystal structure of $4Nb_2O_5.22WO_3$ which was derived directly from the micrograph of Fig. 5. The structure (unit cell outlined) is an intergrowth of two slabs having a single unit-cell width of the TTB type and several unit-cell widths of the ReO_3 type. Pentagonal tunnels occupied by metal–oxygen atoms are shown by open circles. (*b*) Geometrical relation between the structures of $4Nb_2O_5.22WO_3$ and the ReO_3 type. Rotations of groups of the octahedra (enclosed by circles) which occur periodically in the ReO_3-type lattice give rise to the intergrowth structure shown in (*a*). However, this simple operation does not contribute to the occupation of the pentagonal tunnels.

Discussion

Rotation operation

In the preceding section we have already shown the structural relation between the elements of the TTB type and the ReO_3 type. Since the intergrowth

structures that were found in the present study are described by periodic appearances of the elements of the TTB type in the host ReO_3-type structure, they can be formed by a periodic application of the geometrical rotation operation on the ReO_3 type (Hyde & O'Keeffe, 1973). Thus the rotation model seems to be quite attractive for explaining an actual mechanism for the phase transformation to produce the intergrowth structures in solid-state reaction. Firstly we shall consider the intergrowth structures and their disorders in terms of the rotation operation, and then discuss the feasibility of this model for an actual reaction mechanism.

An initial ReO_3-type structure is illustrated in Fig. 6(*b*), where the squares containing crosses indicate the metal–oxygen octahedra. Now we apply the rotation operation on this structure for the case of $4Nb_2O_5.22WO_3$. The groups of octahedra that would be involved in the rotation can be found by inspecting the proposed model for the structure of $4Nb_2O_5.22WO_3$ shown in Fig. 6(*a*), and are encircled in Fig. 6(*b*). In both illustrations an equal number of octahedra are drawn. A regular arrangement of the circles confirms that the periodic rotation operation on the ReO_3 type can produce the structure of $4Nb_2O_5.22WO_3$ if we ignore some of the pentagonal tunnels occupied by metal and oxygen atoms. For the structure of $4Nb_2O_5.50WO_3$ the rotation occurs only in the regions indicated by arrows in Fig. 6(*b*).

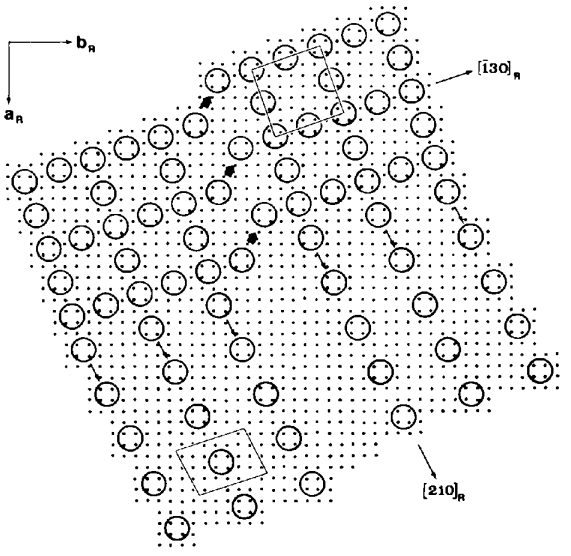

Fig. 7. A schematic illustration of the disordered arrangement of the atoms in the region enclosed by the lines in Fig. 3. The dots represent the metal atoms in the octahedra (see Fig. 2*c*) and the TTB-type elements that occur in the crystal are shown by the encircled dots. The unit cells of $2Nb_2O_5.7WO_3$ (top) and $4Nb_2O_5.22WO_3$ (bottom) are outlined. The antiphase boundary in the region of $2Nb_2O_5.7WO_3$ is explained by displacement of the TTB-type slabs lying parallel to the $[130]_R$ direction. The slabs lying in the $[310]_R$ direction swing to the $[210]_R$ direction at the positions indicated by small arrows, resulting in the new structure of $4Nb_2O_5.22WO_3$. The illustration reveals that the domains of the ReO_3-type separated by the TTB-type slabs are grown coherently.

Let us consider the structural relation between the interface regions of $2Nb_2O_5.7WO_3$ and $4Nb_2O_5.22WO_3$ including some antiphase boundaries and stacking faults shown in Fig. 3. Examination of a structure image corresponding to the area enclosed by lines in Fig. 3 allows us to know the arrangement of the metal atoms in this region. This is illustrated schematically in Fig. 7 using the simplified designation of the ReO_3-type lattice shown in Fig. 2(*c*), where only the positions of metal atoms in the octahedra are shown by dots. The circles indicate the regions where the TTB-type elements occur, and therefore rotation of the octahedra must have taken place. In the region of $2Nb_2O_5.7WO_3$ (the upper half of the drawing) the rows of the TTB-type elements lie along two directions, $[310]_R$ and $[\bar{1}30]_R$. The discontinuity seen in the upper middle of the drawing is generated by a shift of the rows of the TTB-type elements by a vector $2a_R[210]_R$ across the boundary. This vector, shown by solid arrows, corresponds to $a_1[110]$ of the $2Nb_2O_5.7WO_3$ structure, and thus the boundary is considered as an antiphase boundary. In the region of $4Nb_2O_5.22WO_3$ (the lower half of the drawing) the rows of the TTB-type elements are arrayed parallel to the $[210]_R$ direction. The arrangement of the TTB-type slabs near the region of the interface of the two structures is described by swinging the slabs lying in the $[310]_R$ direction of $2Nb_2O_5.7WO_3$ to the $[210]_R$ direction of $4Nb_2O_5.22WO_3$. Their turning points are shown by small arrows in the drawing. The stacking fault in the region of $4Nb_2O_5.22WO_3$ (middle of the drawing) is evidently related to the antiphase boundary in $2Nb_2O_5.7WO_3$ since the TTB-type slabs are continued across the boundary between the two structures. All these disorders can be nicely described by the rotation operation. In other words, the regions of the ReO_3 type which are separated individually by columns of the TTB type are grown coherently throughout the crystal as if they were a perfectly continuous single crystal of ReO_3 type; note that the dots in Fig. 7 form a perfectly periodic arrangement.

As we saw above, the rotation operation is able to explain the geometrical relation between the ReO_3 type and the TTB type not only in the ordered but also in the disordered regions. However, since a simple rotation operation results in no change in composition of the host structure MO_3 after the transformation, it is quite obvious that to explain the observed occupation of some of the pentagonal tunnels, an additional mechanism of diffusion of both metal and oxygen ions for filling the pentagonal tunnels will be required.

It has been suggested (Iijima & Allpress, 1974*b*) that the direct transformation from the ReO_3 type to the

TTB type by the rotation operation may not be feasible. There is more Nb_2O_5 than WO_3 in the starting materials of $19Nb_2O_5.63WO_3$, so that some Nb_2O_5 should be converted into the ReO_3-type structure. Thus we suspected that the actual transformation would take place during the reaction of the involatile species Nb_2O_5 with the vaporized WO_3, which is known to be volatile at the presently used reaction temperature (1620 K) (Blackburn, Hoch & Johnston, 1958). It appears feasible that the regions of ReO_3 type which are observed in the present experiment are not the original WO_3-type starting material but have been reformed after the reaction, as suggested by the electron micrograph shown in Fig. 8. This shows a boundary of two differently oriented regions of ReO_3 type (arrowed) lying parallel to the $[310]_R$ direction. The photograph reveals that the atom arrangement of the boundary is described by a periodic array of imperfect TTB-type elements (see the idealized model in the inset). A similar orientation boundary has been observed previously [see Fig. 2(*a*) of Iijima & Allpress (1974*b*)]. Since these orientation boundaries are in the $[310]_R$ or $[120]_R$ direction, which is in the same as in the TTB-type slabs, they can be considered as growth faults occurring during the reaction. For this reason, the rotation model may not be applied to the formation of TTB-type slabs by converting directly the ReO_3-type structure.

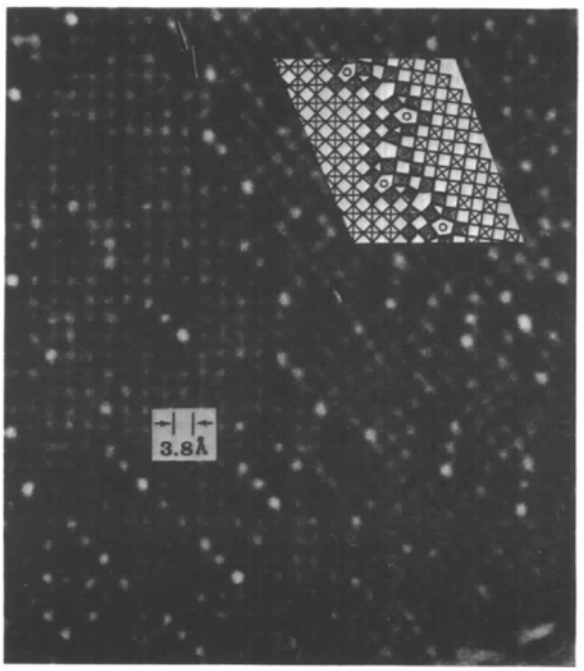

Fig. 8. An orientation boundary of two differently oriented domains of the ReO_3 type that has been formed presumably during recrystallization of the WO_3 starting material. The atomic arrangement near the boundary has a regular array of imperfect TTB-type elements (inset).

Rotation fault and crystallographic shear

In several aspects, the periodic arrays of slabs of TTB-type elements may be compared with the crystallographic shear structures in the ReO_3 type. There is the possibility of occurrence of a homologous series of compounds. This can be produced by varying the separation between the adjacent slabs, as was found in the Magnéli phases. A similar homologous series of compounds was predicted in the compounds of K_xWO_3 by Hussain & Kihlborg (1976). They found that the structure of K_xWO_3 is an intergrowth of two alternating slabs of ReO_3 type and hexagonal-bronze type, so that the series of compounds may be generated by varying the separation of the slabs.

Referring to the structural model of $4Nb_2O_5.22WO_3$ (Fig. 6*a*), the smallest separation would be taken as a half of that in $4Nb_2O_5.22WO_3$ and the positions of the slabs would be indicated by small arrows in Fig. 6(*b*). In this case the structure has a composition $14 \times MO_3$ (octahedra) + $2 \times MO$ (tunnels) = $M_{16}O_{44}$ on the assumption that two out of four pentagonal tunnels in each TTB-type element are occupied by a string of metal–oxygen atoms as we saw in almost all electron micrographs of the TTB-type elements. Therefore, a series of the compounds will be given by multiplication of the a axis of the $M_{16}O_{44}$ structure, *i.e.* the general formula is $M_{14n+2}O_{42n+2}$. Their unit-cell vectors are $a_n = 12{\cdot}01 \times n$, $b_n = 3{\cdot}8$, $c_n = 16{\cdot}99$ Å and $\beta_n = 98{\cdot}13°$. The two compounds that we found in the present study correspond to those with $n = 2$ (for $4Nb_2O_5.22WO_3$) and $n = 4$ (for $4Nb_2O_5.50WO_3$). The hypothetical homologous series of compounds proposed above is also based on the assumption that all the structures have lattice parameters b and c identical with those of $4Nb_2O_5.22WO_3$ and $4Nb_2O_5.50WO_3$, *i.e.* the orientation of the slabs is parallel to $(210)_R$. If the orientation of the slabs is changed, then different types of series of the compounds will be formed. Such a swing of the slabs around the b axis has been found in many crystallographic shear structures in the ReO_3-type structures. Theoretically the hypothetical compounds can range in their composition from $M_{16}O_{44}$ to MO_3. However, as seen in Table 1, one-dimensional crystallographic shear structures become more predominant in a region near MO_3. This suggests that the formation energy of the crystallographic shear would be smaller than that of the TTB-type slabs.

To find a stable arrangement for the crystallographic shear planes, or slab separations, that is also controlled by the composition in a given system, has been a recent interest among solid-state chemists (Iijima, 1975*b*). In order to explain the origin of certain separations of the crystallographic shear planes in the ReO_3-type lattice, Stoneham & Durham (1973) and Iguchi & Tilley (1977) studied theoretically the nature of their ordering using the elastic-continuum theory. Their conclusion is that the lattice strain energy

between two adjacent slabs becomes minimal when they are separated by a certain distance. Their results seem to be in accord with the separation between the slabs of the TTB-type elements. If the lattice strain is a major factor controlling the slab separation, it is then unlikely that the compounds having large c axes would occur in the hypothetical compounds proposed above. A calculation of the lattice strain energy and formation energy for the TTB-type slab structures similar to those for the crystallographic shear structures will provide an answer to the experimental fact that the crystallographic shear structures are favoured over the TTB-type slab structures in the composition range where the two structures are possible (see Table 1).

Regarding interaction forces between the slabs, we made an interesting observation on an imperfect slab where individual TTB-type elements were arrayed irregularly (Fig. 9). The photograph shows a region of $4Nb_2O_5.50WO_3$ containing an irregular spacing of the slabs and a single slab, indicated by an arrow, that is terminated in the middle of the image. As we discussed previously, the TTB-type slabs may have been formed as crystal-growth faults resulting from the vapor transport of WO_3 on the surface of Nb_2O_5. Thus, the TTB-type elements would have been introduced during this solid-state reaction and presumably their location is determined by the interaction of the lattice strain around the TTB-type elements. It is obvious that when a single isolated TTB-type element is generated in the ReO_3-type lattice (see Fig. 2*b*) considerable amounts of displacement of the atoms near the element will take place even though there are no changes in octahedral coordination of the metal atoms. Incidentally, it is also evident that if four pentagonal tunnels of each TTB-type element were empty, the strain field would have fourfold symmetry. However, the occupation of two out of four pentagonal tunnels for each TTB-type element, which may result from the charge balance of the local area of the TTB-type elements, reduces this symmetry to twofold. Perhaps the twofold symmetry of the elements will act to induce their linear arrangement. Now, if the interaction forces between the neighboring elements were negligibly small, they would be formed at random in the ReO_3-type lattice as we saw in Fig. 1(*a*). On the other hand, if the elements were formed in a certain range where their surrounding strain fields could interact with each other, they would be arranged so as to minimize their configuration energies under conditions of thermal equilibrium. The locations and separations of the TTB-type elements in the imperfect slab, shown by circles in Fig. 9, maintain the crystallographic relation with the nearest elements. Such long-range interactions could be explained as a consequence of the interaction of the strain fields, of which the range seems to be around 40 Å in this case. The element indicated by a large arrow in Fig. 9 has a different orientation from the rest of the elements, *i.e.* a pair of the pentagonal tunnels are differently occupied. This can be due to a decreased twofold symmetry interaction with the surrounding elements because of the larger separation. As mentioned earlier, the imperfect arrangement of the TTB elements results from the non-equilibrium nature of our crystals, and thus both the transport of cations and of oxygen ions is equally responsible for the arrangement of the TTB elements.

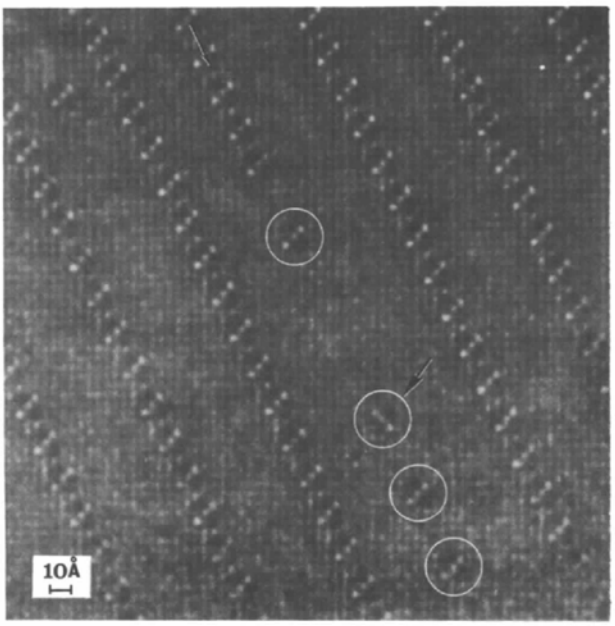

Fig. 9. A high-resolution electron micrograph showing a region of $4Nb_2O_5.50WO_3$. The TTB-type slab (arrowed) is not completely extended, but some isolated TTB elements are formed on the extended area of the slabs. The registered locations of these elements may suggest a long-range interaction acting among the slabs.

I would like to thank Professor J. M. Cowley for his help in the presentation of the manuscript. I acknowledge financial support from the National Science Foundation (DMR-76-06108).

References

ALLPRESS, J. G. (1972). *J. Solid State Chem.* **4**, 173–185.
BLACKBURN, P. E., HOCH, M. & JOHNSTON, H. L. (1958). *J. Phys. Chem.* **62**, 767–773.
HUSSAIN, A. & KIHLBORG, L. (1976). *Acta Cryst.* A**32**, 551–557.
HYDE, B. G. & O'KEEFFE, M. (1973). *Acta Cryst.* A**29**, 243–248.
IGUCHI, E. & TILLEY, R. J. D. (1977). *J. Solid State Chem.* **21**, 49–56.
IIJIMA, S. (1975*a*). *Acta Cryst.* A**31**, 784–790.
IIJIMA, S. (1975(*b*). *J. Solid State Chem.* **14**, 52–65.
IIJIMA, S. & ALLPRESS, J. G. (1974*a*). *Acta Cryst.* A**30**, 22–29.

IIJIMA, S. & ALLPRESS, J. G. (1974*b*). *Acta Cryst.* A**30**, 30–36.
IIJIMA, S. & COWLEY, J. M. (1978). *J. Phys.* (*Paris*), **38**, *Suppl. CF*, 135–144.
IIJIMA, S. & O'KEEFE, M. A. (1978). In preparation.
MAGNÉLI, A. (1953). *Acta Cryst.* **6**, 495–500.
O'KEEFE, M. A., BUSECK, P. R. & IIJIMA, S. (1978). *Nature* (*London*). In the press.
ROTH, R. S. & WADSLEY, A. D. (1965). *Acta Cryst.* **19**, 26–32.
SLEIGHT, A. W. (1966). *Acta Chem. Scand.* **20**, 1102–1112.
STONEHAM, A. M. & DURHAM, R. J. (1973). *J. Phys. Chem. Solids*, **34**, 2127–2135.
WADSLEY, A. D. & ANDERSSON, S. (1970). *Perspect. Struct. Chem.* **3**, 1–58.

Acta Cryst. (1978). A**34**, 931–935

Refinement of Large Structures by Simultaneous Minimization of Energy and *R* Factor

BY A. JACK* AND M. LEVITT

MRC Laboratory of Molecular Biology, University Postgraduate Medical School, Hills Road, Cambridge CB2 2QH, England

(*Received* 29 *March* 1978; *accepted* 22 *May* 1978)

An improved method of crystallographic structure refinement, especially suitable for large molecules, is described. It is based on simultaneous minimization of a realistic potential-energy function and a crystallographic residual. The method has already proved its worth in the final stages of refinement of two structures; an application to crude wire-model coordinates of a small protein is described and evaluated.

Introduction

Until recently the refinement of macromolecular structures against X-ray diffraction data was a laborious process, involving many comparisons of a model with a difference map, followed by manual correction of the model, coordinate idealization, and further refinement. The traditional method, Diamond's (1971) real-space refinement, treats torsion angles (and possibly some bond angles) as variables; it has a wide range of convergence (Diamond, 1976), but suffers from the disadvantage that it is tied to a particular set of 'observed' phases; that is, the function minimized is

$$\int_v (\rho_o - \rho_c)^2 \, dV \equiv \frac{1}{V} \sum_h (F_o - F_c)^2, \qquad (1)$$

whereas we should ideally seek to minimize

$$\Delta = \sum_h (|F_o| - |F_c|)^2. \qquad (2)$$

We can approach this ideal with Diamond's method by using a new map for each cycle, the coefficients of which are $|F_o| \exp(i\alpha_c)$ or $(2|F_o| - |F_c|) \exp(i\alpha_c)$. Nonetheless, this is expensive and still biased toward the starting structure, so that convergence eventually becomes slow.

(2) may be minimized by conventional crystallographic least squares, but only if very high resolution data are available (see, for example, Watenpaugh, Sieker, Herriott & Jensen, 1973). An alternative method is to compute unconstrained shifts, either by least squares or from a difference map, using the gradient/curvature method (Freer, Alden, Levens & Kraut, 1976) to apply these shifts for several cycles, and then to re-idealize the bond lengths and angles. This method also works well with high-resolution (<2 Å) data.

Consider now the problem of refining a rather poorly determined structure, in which atoms may be misplaced by several ångströms. The radius of convergence of least-squares methods is dependent on the data resolution (typically $d/4$ where d is the spacing of the highest-order reflexion). Thus to have any hope of correcting large errors automatically, we must start with low-resolution data. Unconstrained methods are unlikely to work in this case, since the shifts will be so large as to alter the stereochemistry in a way that may not easily be reversed by idealization. The solution is to use a least-squares technique in which constraints (or restraints) on the stereochemistry are included. Two such methods have recently been reported. Konnert (1976) uses Waser's (1963) method to impose quadratic constraints on bond lengths and angles, and solves the resulting sparse set of equations by the method of conjugate gradients. Sussmann, Holbrook, Church & Kim (1977) have used a mixture of constraints and

* Died 14 July 1978.